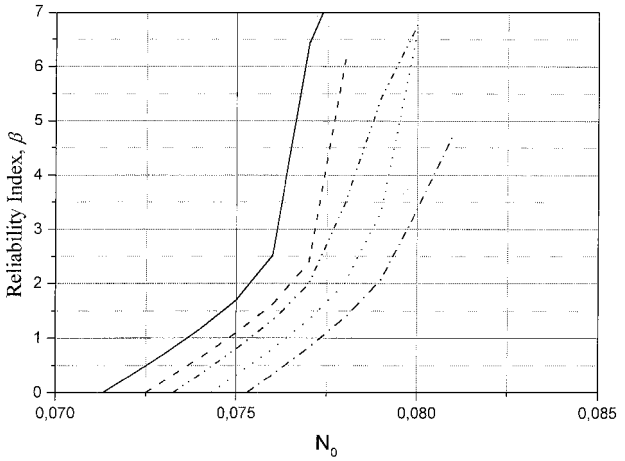

Fig. 1 Comparison of different controllers in terms of probability of not satisfying the project requirements.

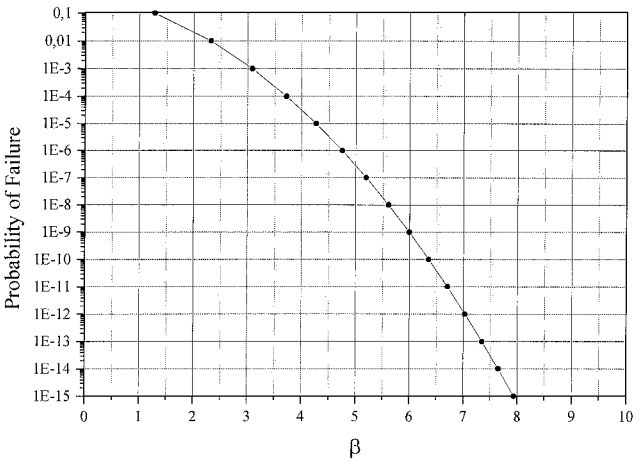

Fig. 2 Relation between the reliability index and the probability of failure.

Obviously, the optimal controller is the one which belongs to S and which minimizes the probability of not complying with the design requirements. A response surface approach was used to relate the values of the aerodynamic derivatives, which are known with uncertainties, to the corresponding value of N_0.

In Fig. 1, the results of the probabilistic analysis are reported in terms of the reliability index β, where the different behavior of the deterministically equivalent controllers may be compared. The relationship between β and the cumulative probability is reported in Fig. 2 for completeness. In particular, Fig. 1 shows the probability of reducing N_0 for the controlled system. The open loop value of N_0 is 0.0874, consequently, all the reported controllers should bring the value of N_0 below approximately 0.07 to comply with the design requirement. As can be seen, different behaviors are obtained for different controllers even though the same N_0 reduction has been achieved in the deterministic case. Obviously, the best controller in the set is the one represented by a continous line. Recalling that N_0 is strictly related to the stresses on the aircraft, this reduction should result in a different behavior of the structure with respect to fatigue performance and, accordingly, should affect aircraft inspection strategies.

Conclusions

The aim of this Note was to study the effects of parameter uncertainties in the design of a control system in order to properly define the design with respect to the satisfaction of the design constraints that the controlled structure should meet. A case study was presented which clearly shows how the use of a probabilistic analysis may help the engineer in evaluating the uncertainties that are inherently present in almost every design. Structural reliability methodologies were used to constitute the probabilistic framework to perform the analysis. The results appear to be promising for obtaining a more rational guideline for project development by properly taking into account the uncertainties in the design variables.

References

[1]Rao, S. S., *Engineering Optimization—Theory and Practice*, Wiley, New York, 1996, Chap. 11.

[2]Ditlevsen, O., and Madsen, H. O., *Structural Reliability Methods*, Wiley, New York, 1996, Chap. 2.

[3]Hasofer, A. M., and Lind, N. C., "Exact and Invariant Second Moment Code Format," *Journal of the Engineering Mechanics Division, ASCE*, Vol. 100, No. 1, 1974, pp. 111–121.

[4]Rackwitz, R., and Fiessler, B., "Structural Reliability Under Combined Random Load Sequences," *Computers and Structures*, Vol. 9, No. 3, 1978, pp. 484–494.

[5]Hohenbichler, M, and Rackwitz, R., "Non-Normal Dependent Vectors in Structural Safety," *Journal of Engineering Mechanics*, Vol. 107, No. 6, 1981, pp. 1227–1249.

[6]Breitung, K., "Asymptotic Approximations for Multinormal Integrals," *Journal of Engineering Mechanics*, Vol. 110, No. 3, 1984, pp. 357–366.

[7]Tvedt, L., "Two Second-Order Approximations to the Failure Probability," Det Norske Veritas, RDIV/20-004-83, Norway, 1983.

[8]Hohenbichler, M., Gollwitzar, S., Kruse, W., and Rackwitz, R., "New Light on First- and Second-Order Reliability Methods," *Structural Safety*, Vol. 4, No. 3, 1987, pp. 267–284.

[9]Schall, G., Gollwitzer, S., and Rackwitz, R., "Integration of Multinormal Densities on Surfaces," *Proceedings of the 2nd IFIP WG 7.5 Working Conference on Reliability and Optimization of Structural Systems*, edited by P. Thoft–Christensen, Springer-Verlag, London, 1988, pp. 235–248.

[10]Box, G. E. P., and Draper, N. R., *Empirical Model-Building and Response Surfaces*, Wiley, New York, 1987, Chap. 1.

[11]Hoblit, F. M., *Gust Load on Aircraft: Concepts and Applications*, AIAA Education Series, AIAA, Washington, DC, 1988, pp. 52–54.

[12]McLean, D., *Automatic Flight Control System*, Prentice–Hall, 1990, pp. 110–118.

A. M. Baz
Associate Editor

Temperature Measurements in a Hypersonic Boundary Layer Using Planar Laser-Induced Fluorescence

P. C. Palma,* S. G. Mallinson,† S. B. O'Byrne,‡
and P. M. Danehy§
Australian National University, Canberra, Australian Capital Territory 0200, Australia
and
R. Hillier¶
Imperial College of Science, Technology, and Medicine, London, England SW7 2BY, United Kingdom

Introduction

THE boundary layer flow over hypersonic vehicles plays a significant role in determining the performance of engine inlets, lifting surfaces, and control flaps. It is therefore critical to have a detailed understanding of relatively simple boundary-layer flows, such as that which develops over a flat plate, to assess possible design input limitations for these systems. One characteristic of hypersonic

Received 2 April 1999; revision received 15 September 1999; accepted for publication 7 October 1999.

*Research Fellow, Department of Physics, The Faculties. Member AIAA.
†Visiting Fellow, Department of Physics; permanent address: Faculty of Engineering, University of Technology Sydney, Broadway, Sydney, New South Wales 2007, Australia. Member AIAA.
‡Graduate Student, Department of Physics. Student Member AIAA.
§Lecturer, Department of Physics. Member AIAA.
¶Professor, Department of Aeronautics.

flows encountered in practical situations is the presence of so-called "real-gas" effects, such as dissociation and vibrational relaxation. These processes can be particularly important in hypersonic boundary layers, where viscous heating can raise the temperature to many times that experienced in the main-stream flow. Despite this fact, there have been few experimental studies of hypervelocity (that is, high-enthalpy and hypersonic) boundary-layer flows where real-gas effects are significant.

Previously, measurements of surface pressure and heat transfer under hypervelocity conditions have been found to agree well with theoretical predictions.[1] In contrast, measurements of the density profile have found an apparent surfeit of density in the boundary layer,[2,3] with compressible boundary-layer theory underpredicting the measurements by up to 50%. At first glance, this would appear to be caused by chemical and vibrational nonequilibrium induced by viscous heating. However, rate calculations indicate that these processes cannot be used to explain the observed discrepancy. Further, experiments on low-enthalpy boundary-layer flows have also measured densities greater than those predicted by boundary-layer theory. A possible explanation for this disagreement is that the measurements were performed using a line-of-sight technique, Mach-Zehnder interferometry. Flow spillage from the sides of the model would therefore have caused the effective optical path length to be smaller than for an ideal two-dimensional flow. The density varies inversely with optical path length, and so spillage would result in higher density being observed.

One way to obtain data which is free from edge effects is to use a technique that gives a cross-section or slice through the flow, such as planar laser-induced fluorescence (PLIF).[4] For this reason, we have performed PLIF thermometry on a hypersonic flow over a flat plate to resolve the discrepancies between experimental boundary-layer profile data and theoretical predictions at hypersonic conditions. The theoretical predictions are calculated with a high-resolution Navier–Stokes solver. The experimental flow is generated using a free-piston shock tunnel.[5] This facility is capable of producing a high-enthalpy, high Mach number freestream flow in which real-gas effects can be appreciable. For this preliminary study, however, we have chosen to focus on a flow condition that is chemically and vibrationally frozen to separate the fluid dynamics from the molecular physics of the flow.

Computational Method

The flow is computed using a high-resolution Navier–Stokes solver, the full details of which are presented elsewhere.[6,7] For the present computations, the flow is treated as a perfect gas with constant ratio of specific heats, $\gamma = 1.4$. The freestream conditions are detailed in the next section. The mesh is 151×81 in the streamwise and transverse directions, respectively. Computations with double the number of cells show only minor differences. The mesh is refined to capture the leading-edge region and wall stretching is applied, which is sufficient to capture the near wall behavior for laminar flows. The computed temperature field for the present flow shows that the boundary layer grows rapidly near the leading edge corresponding to the strong interaction region. By about 10 mm from the leading edge, the boundary layer growth is more gradual, corresponding to the weak interaction region, wherein the experiments were conducted. The temperature rises from the edge of the boundary layer until it reaches a maximum of 1200 K close to the wall. Thereafter, the temperature decreases until it reaches the wall temperature of 295 K, as expected from boundary-layer theory (see, for example, Ref. 3).

Experimental Method

Flow Conditions and Model

The experiments were performed using the T2 free-piston shock tunnel at the Australian National University. A description of the shock tunnel and its operation is given by Stalker.[5] The T2 nozzle has a 15-deg full-angle conical geometry with a 6.4-mm diam throat and nozzle-exit diameter of 73 mm. The primary shock speed was 2.4 km/s, which corresponds to a flow total enthalpy of 5.3 MJ/kg. The nozzle-reservoir pressure was measured to be 27.9 MPa, and the reservoir temperature was calculated to be 4500 K using the equilibrium shock tube code ESTC.[8] The nozzle-exit conditions were calculated using the quasi one-dimensional nonequilibrium nozzle-flow code STUBE.[9] The calculated freestream conditions were: velocity $u_\infty = 2.9 \pm 1\%$ km/s, static temperature $T_\infty = 410 \pm 3\%$ K, static pressure $P_\infty = 5 \pm 8\%$ KPa, density $\rho_\infty = 0.04 \pm 6\%$ kg/m^3, and Mach number $M_\infty = 7.5 \pm 2\%$. The test gas was mostly nitrogen (98.9% N_2 and 1.1% O_2 in the shock tube, resulting in 98.1% N_2, 1.1% NO, 0.4% O_2, and 0.3% O in the test section). The flow at the nozzle exit was both chemically and vibrationally frozen.

The flat plate model is equipped with a sharp leading edge. Its chord and span are 120 and 50 mm, respectively. The model was placed at a zero angle of attack, and the PLIF measurements were made at 75 mm from the leading edge of the flat plate. This corresponded to 50 mm from the nozzle exit, at which position the core flow is approximately 60 mm in diameter. The nozzle-wall boundary layer is laminar, and therefore the temperature and pressure distributions are quite uniform radially to the edge of the core flow. This was confirmed by previous LIF imaging measurements.

Planar Laser-Induced Fluorescence

PLIF is a spectroscopic technique that uses a thin sheet of laser light to excite absorption transitions of a particular chemical species in the flow. Some of the absorbed light is emitted as fluorescence and is collected at right angles to the sheet with an intensified closed-camera-device (CCD) camera. By collecting this signal for two or more different molecular transitions, the two-dimensional rotational and vibrational temperature fields may be evaluated.[4,10] In the current experiment, the sheet enters perpendicular to the flow, with the longest dimension of the cross-section parallel to the flow direction.

Nitric oxide (NO) excitation is employed here because of its well-characterized spectroscopy and desirable properties for thermometry. To eliminate the hazards of handling NO, which is toxic, a small amount of O_2 is added to the nitrogen test gas. Nitric oxide is then produced by chemical reactions in the high-temperature nozzle-reservoir region.

For details of the experimental arrangement, refer to Ref. 10. The output of an excimer-pumped dye laser was frequency doubled to obtain approximately 5 mJ near 226 nm. This wavelength coincides with the (0,0) $A^2\Sigma^+ \leftarrow X^2\Pi$ vibrational transition of NO. Part of the beam was split off for wavelength calibration using LIF in a flame. The remaining laser energy was formed into a laser sheet approximately 0.6 mm thick. The energy measured from a 20 mm section of the laser sheet was typically 600 μJ, which gives an irradiance of 200 kW/cm^2 (assuming a laser pulse duration of 25 ns). The laser linewidth was measured to be 0.18 cm^{-1} by performing LIF in a low-pressure room-temperature cell.

The collection optics are the main difference between the current and previous PLIF experiments.[10] The detection system consisted of an intensified CCD camera (Princeton Instruments; 576×384 pixels) with a Nikon UV lens (focal length 105 mm, $f/4.5$), providing a spatial resolution of about 10 pixels per mm. To improve this, two simple UV lenses were used as a telescope (objective and eyepiece focal lengths 300 and 150 mm, respectively) to increase the magnification. This lens combination imaged a region of 12×8 mm, producing a resolution of 45 pixels per mm. Elastic scatter at the laser wavelength was blocked by using a 3-mm-thick UG5 Schott glass filter.

Spatial calibration was achieved by introducing a small amount of NO into a N_2 bath in the test section and performing PLIF on the static gas sample. A 5-mm-wide section of the laser sheet was blocked, producing a PLIF signal with a known spatial variation. The LIF saturation irradiance I_{sat} was determined by measuring the PLIF signal S_f as a function of laser-sheet irradiance I and assuming $S_f \propto I/(1 + I/I_{sat})$. The $R_2(26.5)$ transition was found to have a saturation irradiance of 178 kW/cm^2. From this measurement, where the static gas conditions were 296 K and 1.35 kPa, the saturation irradiance for other NO transitions and other conditions was estimated. For the current experiments, the level of saturation was approximately 50%. These high levels of irradiance were necessary because of the additional losses introduced by the telescope lenses. Maximum intensifier gain was used for the camera.

One PLIF image is measured for each tunnel run. Five images were obtained for each transition and averaged. The signals were then integrated in the streamwise direction to reduce shot noise. The conditions change in the streamwise direction because of the conical nature ofthe flow, however, over the small region imaged here (8 mm) the variation was negligible. The temperature through the boundary layer is calculated from the ratio of these signals.

Results and Discussion

The measured and calculated rotational temperatures are compared in Fig. 1. It can be seen that the measured temperature falls below the calculated value in the boundary layer, while at the wall, the temperature is greater than that predicted. Also, the boundary layer seems broadened or smeared out in comparison with the calculation. These observations suggest that the spatial resolution of the imaging was insufficient to completely resolve the features of the boundary layer.

While performing PLIF tests on static NO in the test section, we observed that the laser scatter from the surface of the model could be sharply focused to form a 100 μm (two pixel) feature. However, we were unable to achieve a tight focus with the PLIF signal; instead, the sharp edge of the blocked laser sheet was smeared across approximately 0.5 mm. We believe that this reduced resolution is caused by chromatic aberrations from the two extra lenses employed in the telescope. The fluorescence signal is broadband, covering approximately 40 nm, as opposed to the laser scatter which is virtually monochromatic. Hence, we conclude that the current imaging system cannot spatially resolve all of the features in the boundary layer.

To verify that the discrepancy between theory and experiment is indeed because of the blurring of the signal, a blur function was determined from the PLIF tests on static NO in the test section. This blur function is a measure of how much the actual measurement system varies from an ideal imaging system, which has perfect resolution. By measuring this blur function and convolving it with the theoretical curve, we can determine if the descrepancies in Fig. 1 are indeed mainly because of the imaging system. It is important to note that deconvolving the true temperature profile from the measured signal was not possible because high-frequency information has been lost in the measurement process, especially at the wall where the true profile stops abruptly.

The blur function was determined to be a Gaussian function with a full width at half maximum of 0.6 mm. This blur function was convolved with the theoretical temperature profile to account for imperfections in the imaging system. Figure 2 shows the comparison between the blurred theoretical profile and the measured temperature profile. The agreement is very good, which implies that the discrepancies indicated in Fig. 1 are largely because of imperfections in the imaging system.

Considering the previous measurements,[2,3] the minimum density in the boundary layer (which occurs at the same location as the maximum temperature) was double that predicted by boundary layer theory. The pressure across the boundary layer will be very nearly constant, and so this corresponds to predicting a maximum temperature twice that observed in experiment. The present observations therefore imply that the line-of-sight measurement technique em-

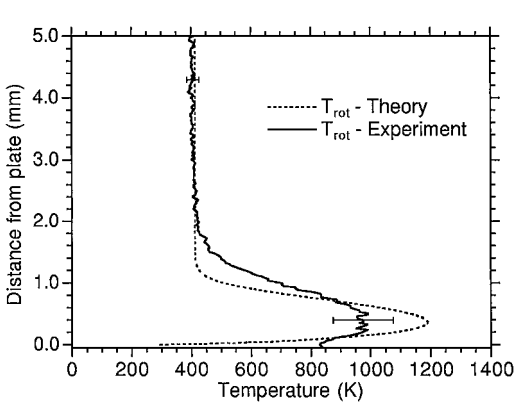

Fig. 1 Temperature as a function of distance normal to the flat plate.

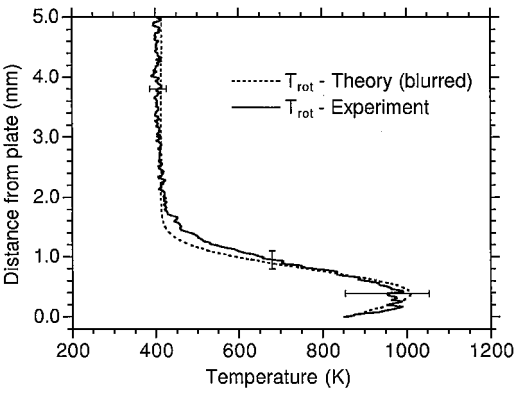

Fig. 2 Comparison between blurred theory and measured temperature.

ployed in the earlier studies, namely Mach-Zehnder interferometry, was affected by flow spillage at the edges of the plate. The PLIF technique, which captures a two-dimensional slice through the flow, does not suffer from this problem.

The two transitions used here, ${}^{O}P_{12}(2.5)$ and $P_1(35.5)$, allow excellent temperature sensitivity because of the large difference in the energies ($\Delta E = 2028$ cm^{-1}) of their absorbing rotational levels. The error in the temperature can be determined from $\delta T/T = \delta R/R \times kT/\Delta E$, where R is the ratio of the two fluoresecence signals, $k = 0.695$ K^{-1} cm^{-1} is the Boltzmann constant, and T is the rotational temperature. The main sources of uncertainty in this experiment are laser-mode fluctuations, laser-beam attenuation by absorption, and saturation of the molecular transition. The pulse-to-pulse variation in the PLIF signal because of mode fluctuations is about 25% at the conditions encountered in the freestream. By averaging five images for each transition, and using the favorable value of $\Delta E/kT$ (7.1 in the freestream and 2.4 in the boundary layer), the uncertainties are significantly reduced. The uncertainty in the measured temperature because of mode fluctuations is ±2.5% in the freestream and ±7.4% in the boundary layer.

Extensive modeling of the expected PLIF signals was performed before the experiments to choose the optimal transitions that reduce uncertainties because of beam absorption and saturation. As mentioned, the conditions along the laser path length are reasonably uniform and can be approximated by a 30-mm uniform region at the freestream conditions. The signals from the low-J and high-J lines decrease by 12 and 0.07%, respectively, over this distance, which causes the measured freestream temperature to be systematically high by 1.7% after 30 mm. Continuing this calculation into the boundary layer produces a systematic error of +4% at 1200 K. If saturation were included in these calculations, the uncertainties because of beam absorption would be significantly reduced.

Both transitions are single and isolated and therefore should have the same saturation behavior as the irradiance is varied. If both transitions have the same level of saturation, then the saturation factor $(1 + I/I_{sat})^{-1}$ will cancel when determining the temperature from the signal ratio. The B-coefficients for the low-J and high-J lines are 147.0 and 166.5 s^{-1}(W/cm^2/cm^{-1})$^{-1}$, respectively, so the irradiance for the high-J line was made ~12% less. Using the measured laser irradiances, the systematic errors because of incomplete cancellation of this saturation term is estimated to be +0.16 and +0.6% in the freestream and boundary layer, respectively. Combining all the uncertainites gives systematic errors of +7 and +50 K, and random errors of ±10 and ±90 K, in the freestream and boundary layer, respectively. The use of partially saturating laser irradiances introduces a novel extension to the current use of PLIF in the linear regime. The higher irradiances afforded by this partially saturating approach produces much higher signal levels.

Conclusions

Temperature measurements in a chemically and vibrationally frozen hypersonic laminar boundary layer have been presented. The measurements show good agreement with the predictions from a high-resolution Navier–Stokes solver. The success of this

preliminary study indicates that more extensive measurements are feasible. In particular, the study of real-gas effects on boundary layers can now be undertaken with reasonable confidence in the PLIF measurement system. However, improvements to the imaging system (to reduce chromatic aberrations) are necessary to resolve flow features less than 0.5 mm in size. The use of partially saturated fluorescence signals is a novel extension to the generally-used linear PLIF technique. In conclusion, this study would seem to indicate that the discrepancies previously observed between measured and calculated density profiles[2,3] are most likely because of flow-spillage affecting the line-of-sight measurement technique.

References

[1]Mallinson, S. G., Gai, S. L., and Mudford, N. R., "The Interaction of a Shock Wave with a Laminar Boundary Layer at a Compression Corner in High Enthalpy Flows Including Real Gas Effects," *Journal of Fluid Mechanics*, Vol. 342, No. 2, 1997, pp. 1–35.

[2]Baird, J. P., Lyons, P. R. A., and Gai, S. L., "Density and Velocity Profiles in Nonequilibrium Laminar Boundary Layers in Air," AIAA Paper 85-0976, 1985.

[3]Mallinson, S. G., Gai, S. L., and Mudford, N. R., "The Boundary Layer on a Flat Plate in Hypervelocity Flow," *Aeronautical Journal*, Vol. 100, No. 2, 1996, pp. 135–141.

[4]Eckbreth, A. C., *Laser Diagnostics for Combustion Temperature and Species*, 2nd ed., Gordon and Breach, 1996.

[5]Stalker, R. J., "A Study of the Free-Piston Shock Tunnel," *AIAA Journal*, Vol. 5, No. 12, 1967, pp. 2160–2165,

[6]Hillier, R., Kirk, D., and Soltani, S., "Navier–Stokes Computations of Hypersonic Flows," *International Journal of Numerical Methods in Heat and Fluid Flow*, Vol. 5, No. 3, 1995, pp. 195–211.

[7]Mallinson, S. G., Hillier, R., Zanchetta, M., Soltani, S., and Kirk, D., "An Experimental and Numerical Study of Hypersonic Turbulent Boundary Layers," AIAA Paper 97-2290, June 1997.

[8]McIntosh, M., "Computer Program for the Numerical Calculation of Frozen Equilibrium Conditions in Shock Tunnels," Rept., Dept. of Physics, Faculties, Australian National Univ., Canberra, Australian Capital Territory, Australia, 1968.

[9]Vardavas, I., "Modelling Reactive Gas Flows Within Shock Tunnels," *Australian Journal of Physics*, Vol. 37, 1984, pp. 157–177.

[10]Palma, P. C., Danehy, P. M., and Houwing, A. F. P., "Non-Intrusive Thermometry in Shock Layers Using Multi-Line Fluorescence Imaging," *21st International Symposium on Shock Waves*, Panther Publishing, Canberra, Australian Capital Territory, Australia, 1997, pp. 447–452.

R. P. Lucht
Associate Editor